



# Investigating the Mechanism of Facet Formation and the Influence of Crack Initiation Size on a Cast Aluminum Alloy in Ultrasonic Fatigue Under Varied Humidity Environments

W. Li<sup>1</sup> · L. Shi<sup>1</sup> · Y. Shi<sup>1</sup> · X. Su<sup>1</sup>

Received: 10 July 2023 / Accepted: 1 November 2023 / Published online: 20 November 2023  
© Society for Experimental Mechanics 2023

## Abstract

**Background** Extensive research was conducted to analyze the ultrasonic fatigue behavior of ASGU-T64 cast aluminum alloy under different humidity environments. The study placed particular emphasis on investigating the factors influencing crack initiation, as well as the propagation of both short and long cracks. By examining the alloy's performance in various moisture conditions, a comprehensive understanding of its fatigue behavior was achieved.

**Objective** The primary objective is to elucidate the mechanism underlying crack initiation and accurately predict the lifespan of short and long cracks. The ultimate goal is to determine how crack initiation size affects the percentage of crack initiation life in relation to the overall fatigue life.

**Method** Scanning Electron Microscope (SEM) and Electron Back Scatter Diffraction (EBSD) were employed and provided valuable insights into the characteristics of the facets. Furthermore, computational methods were utilized, employing the Paris crack growth law, to accurately determine the growth lives of both short and long cracks. By combining experimental and computational approaches, a comprehensive understanding of the fracture behavior and crack growth mechanisms was achieved, contributing to the advancement of knowledge in this field.

**Results** Through this study, it was discovered that fatigue cracks in the AS7GU-T64 alloy consistently initiated on the surface of the sample, primarily due to the presence of persistent slip bands (PSBs). Each facet observed on the fracture surface corresponded to an entire grain within the short crack area. While the stress intensity factor fell within the range of 3.5 to 10 MPa·√m for all three environments, it was found that the stress intensity factor in dry air exceeded that of saturated air and distilled water conditions. Importantly, the percentage of fatigue life attributed to crack initiation was found to be heavily dependent on the humidity of the testing environment and the applied stress amplitude. These insights highlight the intricate relationship between environmental conditions, stress intensity factor, crack initiation, and the overall fatigue life of the AS7GU-T64 alloy.

**Conclusion** Humidity negatively affects the ultrasonic fatigue life of the AS7GU-T64 alloy. Furthermore, the size of crack initiation was identified as a significant factor influencing the percentage of crack initiation life in relation to the overall fatigue life.

**Keywords** Ultrasonic fatigue · Cast aluminum alloy · Facet formation · Life prediction · Crack initiation life

## Introduction

Cast aluminum alloys are largely used in automotive industry because of their low density, high strength/weight ratio and good corrosion resistance. Some components in vehicle

like engine head and cylinder block experience more than  $10^8$  alternative cycles in their service life. As the number of cycles to failure is very large, in the VHCF regime, the component needs to be designed to endure until  $10^9$  or even  $10^{10}$  cycles under similar loading conditions. Ultrasonic fatigue testing has attracted more and more people's attention due to its high testing frequency (20 kHz). With this testing technique, the fatigue stress-life (S–N curves) data generation can be greatly accelerated [1, 2]. Therefore, it is vital to better understanding the fatigue properties of aluminum alloys in the very high cycle regime.

✉ Y. Shi  
shiyd@hzcu.edu.cn

<sup>1</sup> Zhejiang Provincial Engineering Center of Integrated Manufacturing Technology and Intelligent Equipment, Hangzhou City University, Hangzhou 310015, Zhejiang, China

**Table 1** The chemical composition of AS7GU-T64 (by weight)

Al	Si	Cu	Mg	Fe	Ti	Mn	Sr
Bal	7.04	0.48	0.36	0.11	0.14	0.06	0.03

Most of the testing data regarding the VHCF are conducted based on ultrasonic fatigue testing instrumentation. Engler-Pinto et al. [3] found out that for a cast aluminum, environment humidity has a great impact on the fatigue life obtained at ultrasonic frequency. Wei, Weir and Stanzl-Tschegg [4–6] have shown that crack growth rate can be accelerated in the presence of humidity and this phenomenon attributed to hydrogen embrittlement. Zhu et al. [7] observed similar results for E319 cast aluminum that longer ultrasonic fatigue life in lab air compared to ultrasonic fatigue tests submerged in water. Numerous studies [8–10] have shown that porosity has the most significant effects on the fatigue strength in HCF and VHCF regime, because it usually acts as a preferential crack initiation site. Paris et al. [11] developed Paris-Hertzberg-McClintock crack growth rate law and found out that crack initiation life is a significant portion of total fatigue life instead of crack growth life in VHCF regime. Nakasone and Hara [12] have used FEM method to simulate the crack growth life and obtained same conclusion that crack growth life is in the range of  $10^2$ – $10^5$  cycles which is negligible compared to crack initiation life. However, contrary to the previous researchers, Omata [13] observed that crack propagation life is a dominate portion in total fatigue life if crack originated from an inclusion.

In this study, a thorough examination of the fracture surfaces was conducted using SEM. Special attention was given to identifying the areas of crack initiation, as well as the regions associated with short and long crack growth. With regards to crack initiation, the mechanisms involved in the formation of facets were carefully considered. In addition, predictions were made regarding the portions of crack initiation and crack propagation life.

**Table 2** The mechanical property of AS7GU-T64

E (GPa)	Yield strength (MPa)	Ultimate strength (MPa)	Elongation (%)
77.8	210	294	7.8

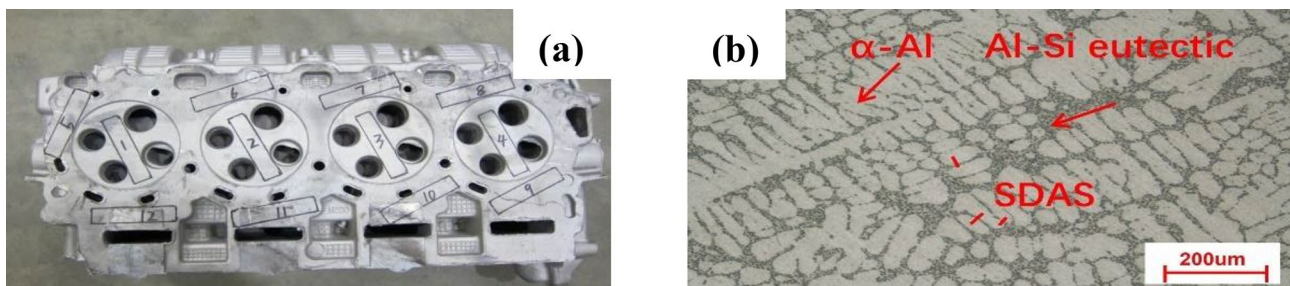
## Experimental Details

### Material and Tensile Test

The cast aluminum alloy in the present study is designated as AS7GU and the chemical composition is detailed in Table 1. The test samples were extracted from brand new cylinder heads, as illustrated in Fig. 1(a). Figure 1(b) shows the typical microstructure of the material, which consists of primary alpha-aluminum and Al-Si eutectic structure. The surface material underwent rapid quenching, resulting in a high solidification rate. As a result, the secondary dendrite arm spacing (SDAS) is small and the presence of casting defects such as pores, oxide films, and non-metallic inclusions is nearly absent. It is important to note that the severe loading conditions only apply to the surface material. All 12 samples were extracted from the surface of the cylinder head, and their respective locations are marked in Fig. 1(a).

The tensile mechanical properties at room temperature are summarized in Table 2. The Young's modulus was determined by subjecting all specimens to cyclic loading at a frequency of 1 Hz and an amplitude of  $\pm 30$  MPa for 10 cycles; the average value for all the samples is reported in Table 2. The SDAS (23 $\mu$ m) was measured by Image Pro software on a 500mm<sup>2</sup> finely polished area (up to 1 $\mu$ m oxide aluminum powder), and over 100 measurements were conducted for each average value.

The geometry of ultrasonic fatigue sample is illustrated in Fig. 2. To minimize manufacturing residual stress, a low stress turning technique was employed during the machining process of ultrasonic fatigue specimens. After machining, all specimens underwent longitudinally polishing using 600 grit abrasive paper achieve a surface roughness (Ra) of less than 0.2 $\mu$ m.

**Fig. 1** (a) Brand new cylinder head, (b) Microstructure of AS7GU-T64

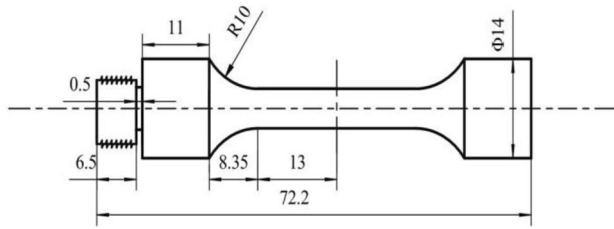


Fig. 2 Geometry of ultrasonic fatigue test specimen

### Ultrasonic Fatigue Test

Ultrasonic fatigue test was conducted using a fatigue test machine which was developed by the Institute of Physics and Materials Science, University of BOKU, Vienna, Austria, as shown in Fig. 3. The key component of ultrasonic fatigue testing machine is ultrasonic transducer, which converts the sinusoidal voltage signal into mechanical movement at a frequency of 20 kHz using piezoelectric ceramic. The amplitude of this mechanical movement was then amplified by an ultrasonic horn, which has a continuously reduced cross section. The amplified vibration waves were directed into the specimen and reflected by the opposite end. When the resonance frequency of specimen matches 20 kHz, the injected and reflected waves will superimpose to create a resonant vibration. More comprehensive information on ultrasonic fatigue testing can be found in references [14–16]. All specimens were subjected to fully reversed loading condition ( $R = -1$ ). To ensure that specimen temperature remained below 25°C, ultrasonic loading is applied in well-control pulses, with a 200 ms on/2000 ms off cycle.

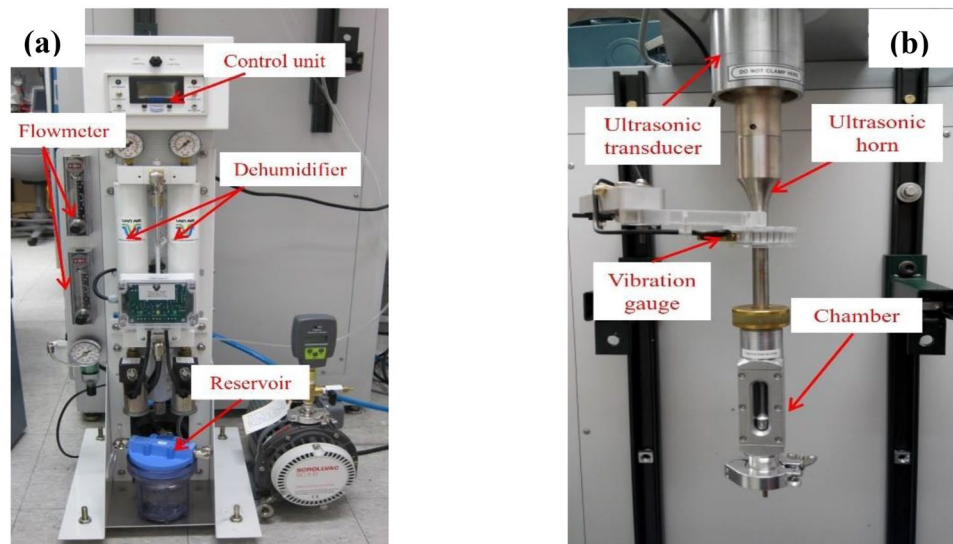
A specially designed device, as depicted in Fig. 3(a), was utilized to generate dry air and saturated air for the experimental conditions. Compressed air was injected into a humidity generator, and a controlled volume of dry air was directed into a water reservoir to create saturated air. By adjusting the volume ratios of the dry air and saturated air, air with varying levels of humidity could be produced. In order to conduct ultrasonic fatigue testing in distilled water, the specimens were submerged in the water. To ensure that the environmental conditions did not interfere with the system's vibrations, an environmental chamber was positioned at the neutral node point of the lambda rod, as illustrated in Fig. 3(b).

### Results and Discussion

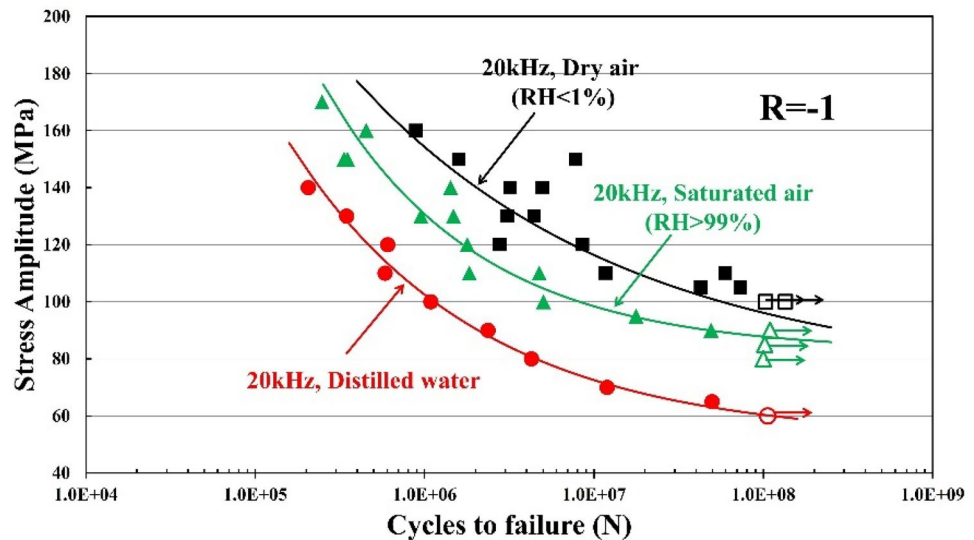
#### S-N Curves

Figure 4 illustrates the S-N curve for the ultrasonic fatigue testing of AS7GU-T64 alloy under various humidity levels. The specimens that did not fail, also known as run-outs, are indicated by arrows pointing to the right. The solid lines represent the medium S–N curves, which were determined using the random fatigue limit (RFL) model [3, 17]. It is evident from the results that ultrasonic fatigue testing conducted in dry air exhibited the highest fatigue life, while testing performed in distilled water resulted in the lowest fatigue life. This clearly indicates that humidity has a detrimental effect on the ultrasonic fatigue life of this particular alloy. These findings are consistent with the previous research conducted by Engler-Pinto et al. [3], Zhu et al. [7], and Stanzl-Tschegg et al. [18], who also observed a decrease in

Fig. 3 (a) Humidity air generator, (b) Ultrasonic fatigue testing system



**Fig. 4** AS7GU-T64 ultrasonic fatigue test results in various humidity levels



ultrasonic fatigue life for cast aluminum alloys with increasing humidity.

### Crack Initiation and Facets Formation Mechanisms

For this study, all specimens were carefully extracted from the deck surface of a high-performance cylinder head. It is important to note that these specimens were characterized by very low levels of casting defects, such as porosity, oxides, and non-metallic inclusions. The absence of such defects, which can potentially serve as crack initiation sites, led to the occurrence of all fatigue cracks initiating from the surface of the specimens. This initiation mechanism primarily involved the formation of slip facets, as illustrated in Fig. 5.

Figure 6 presents the fracture surface of selected specimens subjected to ultrasonic frequency testing under various humidity environments. It is apparent that a significant number of facets are formed along the crack propagation path, particularly in specimens tested under dry air conditions as illustrated in Fig. 6(a) and (b). Conversely, the presence of facets decreases notably in tests conducted using saturated air and distilled water. Notably, these facets tend to be located in close proximity to the fatigue crack initiation site, highlighting that their formation predominantly occurs during the short crack propagation stage.

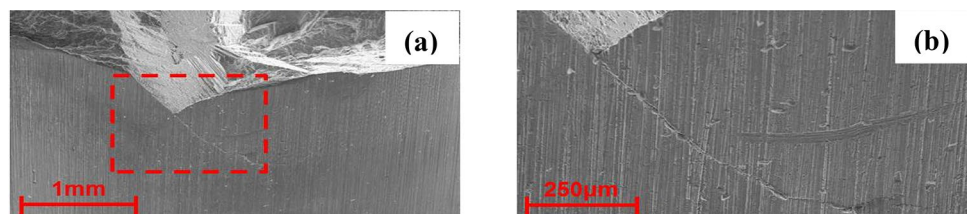
To gain a deeper understanding of these facets, certain specimens that did not fully separate during the fatigue

test were sectioned and polished. This allowed for the exposure of the fatigue crack path, as depicted in Fig. 7. The observed facets on the fracture surfaces were found to form an angle approximately 45 degrees relative to the loading direction, which corresponds to the maximum shear stress direction.

Research conducted by Zhu et al. [7], Miao et al. [19], and Tiryahioğlu et al. [20] provides evidence that facets in differing materials could potentially originate from slip bands. To inspect the characteristics of the facets in this current examination, an Electron Backscattered Diffraction (EBSD) analysis was carried out, with the results demonstrated in Fig. 8. Figure 8(a) and (c) displays SEM images with the facets marked by red arrows. Figures 8(b) and (d) showcase the corresponding inverse pole maps that were obtained from the EBSD analysis, with varying colors representing different crystallographic orientations, or in other words, different grains. Observation drawn from Fig. 8 indicates that the facets are consistently located within the grains, thereby eliminating the hypothesis of the facets corresponding to twin boundaries. Specifically, Figs. 8(c) and (d) illustrate a slip facet that traverses an entire grain; this is then succeeded by the propagation of the fatigue crack along the grain boundary, moving from left to right in the particular image.

According to Zhu et al. [21] and Wei [5], it has been demonstrated that the rate of crack propagation is not

**Fig. 5** (a) SEM of the crack initiation site, (b) Magnified view of boxed area



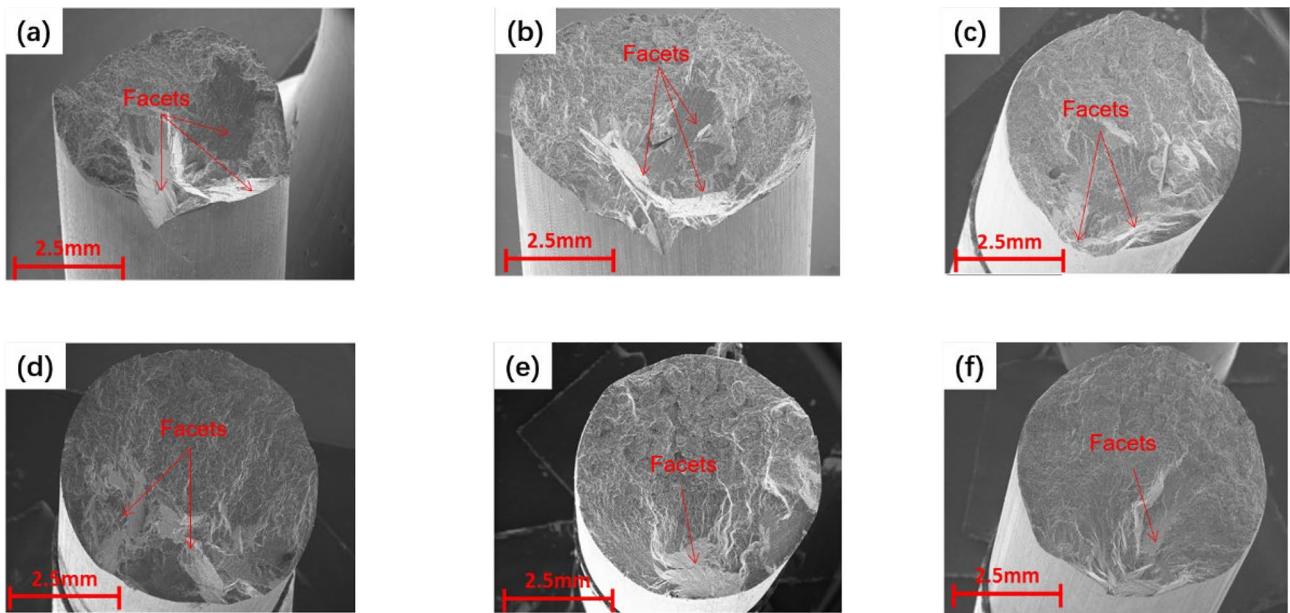


**Fig. 6** Fracture surfaces of ultrasonic specimens tested in different environment. (a) 110 MPa in dry air, (b) 130 MPa in dry air, (c) 110 MPa in saturated air, (d) 130 MPa in saturated air, (e) 110 MPa in distilled water, (f) 130 MPa in distilled water

solely dependent on the stress intensity factor, but also influenced by the humidity of the environment. Wei proposed that the effect of humidity can be quantified using

the "water exposure" term, represented by the ratio of water vapor pressure ( $P$ ) to the testing frequency ( $f$ ). It is evident that an increase in environmental humidity leads

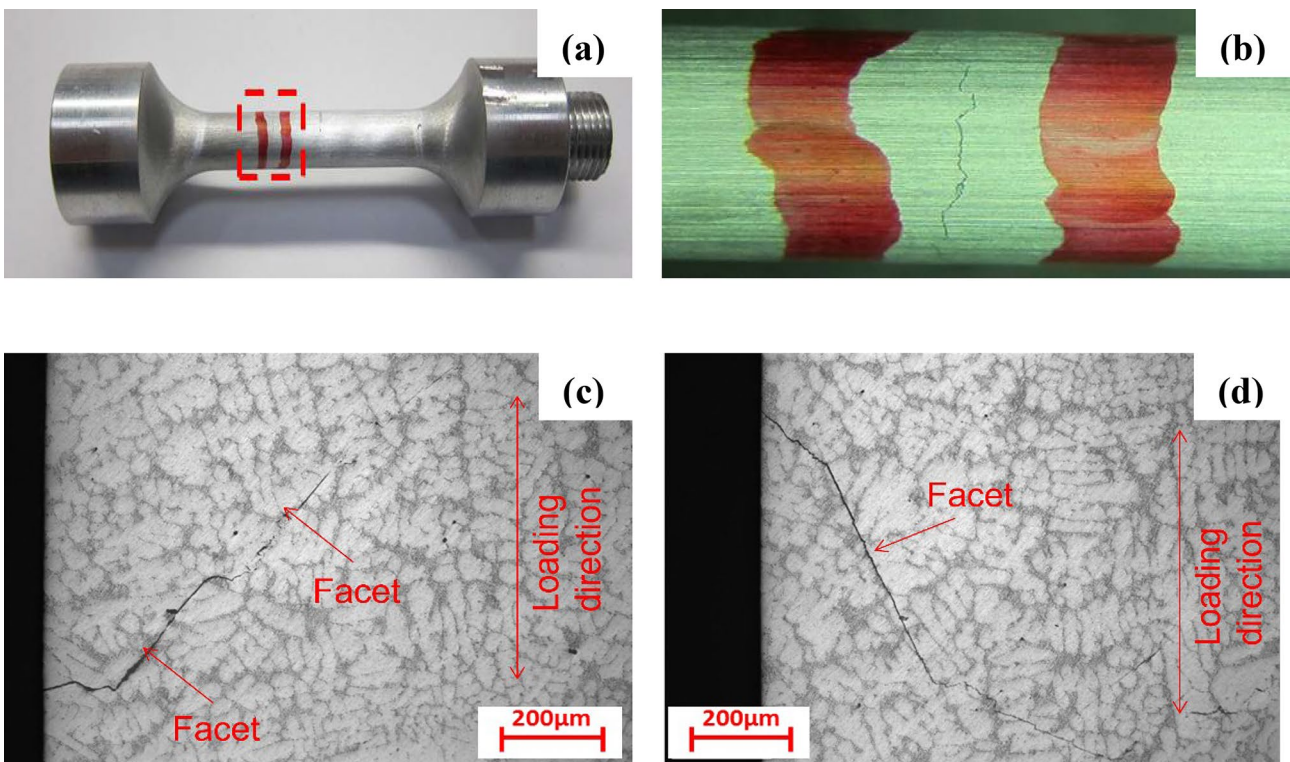
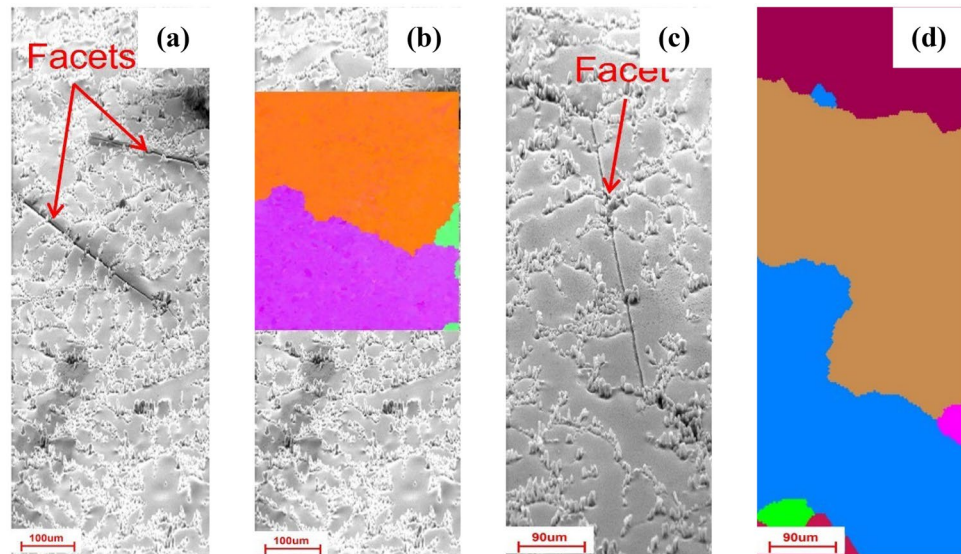


**Fig. 7** (a) The failed sample from ultrasonic fatigue with a crack on the surface. (b) A magnified view of the area where the crack occurred. (c) and (d) are polished cutting surfaces

**Fig. 8** (a) and (c) are SEM pictures, (b) and (d) are inverse pole maps from EBSD analysis



to a higher rate of crack propagation and a decrease in the percentage of facets.

In all the ultrasonic fatigue tests conducted in various humidity environments, the fatigue crack consistently originated from the surface of the specimen. Drawing upon the present investigation and previous studies [21, 22], a probable explanation for the formation of facets can be summarized as follows:

- During cyclic loading, localized cyclic plastic deformation occurs, leading to the formation of persistent slip bands (PSBs) on grains that are favorably oriented with respect to the loading direction (slip system oriented close to the maximum shear stress direction).
- Fatigue crack initiation takes place at these PSBs, causing stress concentration at the crack tip and leading to the formation of a cyclic plastic zone.
  1. In the early stage of crack, the average crack growth rate within the initiation area can be as low as  $10^{-12}$  m/cycle [18]. Cyclic plastic deformation accumulates ahead of the crack tip, resulting in the development of slip facets. The crack then "jumps" to the next grain;
  2. Once the crack length reaches a threshold value and the crack propagation rate becomes sufficiently high, the accumulated cyclic deformation no longer causes the crack to propagate through the slip plane. Consequently, slip facets do not form, and the crack propagates through traditional fatigue mechanisms (such as striation formation);
- The presence of water at the crack tip accelerates the crack propagation rate

1. In tests performed under 20 kHz and dry air, the absence of humidity significantly reduces the crack propagation throughout the test, resulting in long fatigue lives and higher percentage of facets;
2. However, when tests are conducted at 20 kHz and humidity, is a corresponding reduction in fatigue life and the percentage of facets. This is because higher humidity promotes a higher crack propagation rate;

### Quantitative Evaluation of Short and Long Crack Growth Region

The fracture can be categorized into four parts: crack initiation area, short crack growth area, long growth area and final fracture area, all based on the facet feature, as shown in Fig. 9. The crack initiation region is characterized by small facets that are formed as a result of the mechanisms related to PSBs. On the other hand, the short crack growth region is distinguished by large facets, which are formed when the crack propagates through an entire grain. Each facet in this region corresponds to a grain. In contrast, the long crack growth region is identified by the presence of river lines, which are similar to other crack growth areas observed in samples that failed due to High Cycle Fatigue (HCF).  $a_0$  and  $a_i$  are the length of short crack growth area where large amounts of facets were formed and long crack growth area in the crack propagation direction, respectively. For all the specimens, the fracture surfaces were carefully examined and the value of  $a_i$  and  $a$  were measured accordingly. Since all the cracks were initiated from the surface through the mechanism of PSBs, both the starting points of  $a_0$  and  $a$  were located on the surface.

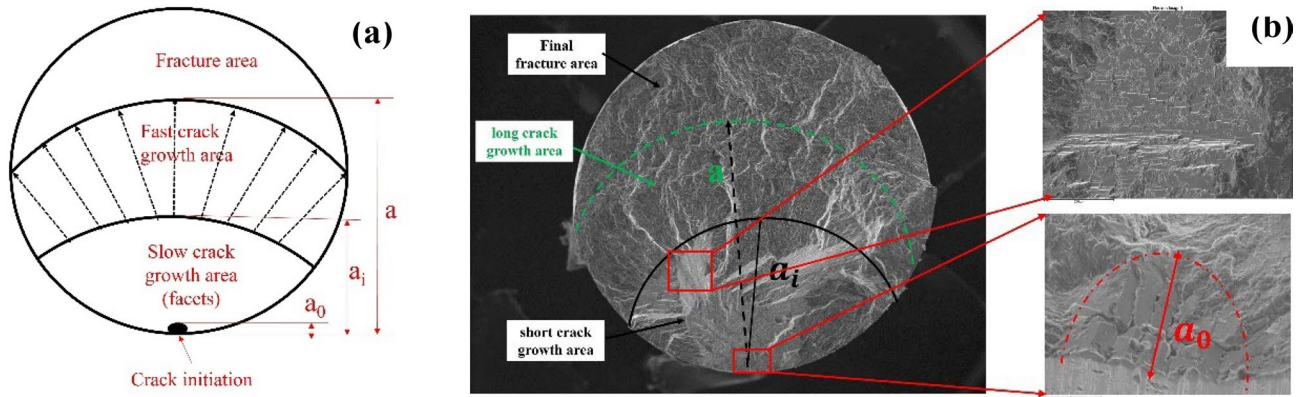


**Fig. 9** (a) Diagram showing the semi-circular fatigue crack growth from  $a_0$  to  $a_i$  and finally  $a$ . (b) Short and long crack area features and measurements of  $a_0$  for specimen fatigued at 130 MPa in distilled water

### Fatigue Life Prediction

It is reasonable to make the hypothesis that the total fatigue life can be divided into three parts which are associated with (1) micro-crack initiation life ( $N_{int}$ ), (2) stable micro-crack propagation life ( $N_{a_0-a_i}$ ) and unstable macro-crack propagation life ( $N_{a_i-a}$ ), respectively.

$$N_{total} = N_{int} + N_{a_0-a_i} + N_{a_i-a} \quad (1)$$

Since the stable micro-crack and unstable macro-crack propagation life can be estimated by Paris-Hertzberg-McClintock crack growth law [11],

$$\frac{da}{dN} = b \left( \frac{\Delta K_{eff}}{E\sqrt{b}} \right)^3 \quad (2)$$

where  $a$  is the crack length,  $N$  is the cycle number,  $b$  is the magnitude of the Burger’s vector,  $\Delta K$  is the effective stress intensity factor, and  $E$  is the Young’s modulus.

The effective stress intensity for semi-elliptical crack,  $\Delta K_{eff}$ , can be calculated as follows [23]:

$$\Delta K_{eff} = 0.65\sigma_a \sqrt{\pi a} \quad (3)$$

Since the driving force for crack propagation under cyclic loading is primarily influenced by the tension part of the load, the amplitude of stress (instead of range of cyclic load) was used to calculate the effective stress intensity factor in the present paper.

#### Estimation of short crack growth life portion, from $a_0$ to $a_i$

At the beginning of stable crack propagation (the threshold corner of crack growth curve), equation (2) yields.

$$\frac{da}{dN} = b \text{ and } \frac{\Delta K_0}{E\sqrt{b}} = 1 \text{ or } \frac{a_0}{b} = \frac{E^2}{0.65^2 \pi (\Delta\sigma)^2} \quad (4)$$

where  $\Delta K_0$  denotes the stress intensity factor of crack size  $a_0$ .

The fatigue life consumed from  $a_0$ , the initiated crack size, to  $a_i$ , the transition point from short to long crack, can be determined by integration the crack growth law, equation (2) and we can obtain:

$$\frac{da}{dN} = b \left( \frac{\Delta K_{eff}}{E\sqrt{b}} \right)^3 = b \left( \frac{\Delta K_0}{E\sqrt{b}} \right)^3 \left( \frac{a}{a_0} \right)^{\frac{3}{2}} = b \left( \frac{a}{a_0} \right)^{\frac{3}{2}} \quad (5)$$

and integrating this equation with short crack limits, from  $a_0$  to  $a_i$ , give us:

$$N_{a_0-a_i} = \frac{(a_0)^{\frac{3}{2}}}{b} \int_{a_0}^{a_i} \frac{1}{a^{\frac{3}{2}}} da = \frac{2a_0}{b} \left( 1 - \sqrt{\frac{a_0}{a_i}} \right) \quad (6)$$

Substituting equation (4) into equation (6), we can get an expression which can be used to calculate the fatigue portion consumed by short crack propagation, from the threshold corner,  $a_0$ , up to the transition point denoted by  $a_i$ :

$$N_{a_0-a_i} = \frac{4.73E^2}{\pi(\Delta\sigma)^2} \left( 1 - \sqrt{\frac{a_0}{a_i}} \right) \quad (7)$$

#### Estimation of long crack growth life portion, from $a_i$ to $a$

According to the ASTM standard [24], it has been reported that in the short crack propagation area, the crack growth rate can be significantly higher than in the long crack propagation area, even when the nominal driving force is the same, primarily due to the absence of crack closure effect. As a result, the crack growth rate in area ( $a_i$  to  $a$ ) reduced by a factor of “1/3<sup>3</sup>” [25],

compared to crack growth rate in area ( $a_0$  to  $a_i$ ). Hence, substituting the factor into the crack growth law formula, we can obtain:

$$\frac{da}{dN} = \frac{b}{x^3} \left( \frac{\Delta K}{E\sqrt{b}} \right)^3 \left( \frac{a}{a_0} \right)^{\frac{3}{2}} = \frac{b}{x^3} \left( \frac{a}{a_0} \right)^{\frac{3}{2}} \quad (8)$$

and integrating crack growth law from a semi-elliptical crack size  $a_i$  to final crack size  $a$ , give us:

$$N_{a_i-a} = \frac{x^3(a_0)^{\frac{3}{2}}}{b} \int_{a_i}^a \frac{da}{a^{\frac{3}{2}}} = \frac{2a_0}{b} \left[ x^3 \sqrt{\frac{a_0}{a_i}} - x^3 \sqrt{\frac{a_0}{a}} \right] \quad (9)$$

As  $\frac{a_0}{b}$  is given by equation (4) and finally we can get the formula which can calculate the number of cycles consumed by a semi-elliptical surface crack, from transition point,  $a_i$  to the final failure size,  $a$ :

$$N_{a_i-a} = \frac{4.73E^2}{\pi(\Delta\sigma)^2} \left[ x^3 \sqrt{\frac{a_0}{a_i}} - x^3 \sqrt{\frac{a_0}{a}} \right] \quad (10)$$

The fatigue life for the crack initiation can be predicted as  $N_{int} = N_f - N_{a_0-a_i} - N_{a_i-a}$ . Previous studies [26] have

observed that the factor of  $x$  is approximately 3 for low stress ratios ( $R < 0$ ) and 1 for high stress ratios ( $R > 0.8$ ). Therefore, in this study, we assign the value of  $x$  as 3.

The predicted fatigue crack initiation, propagation life and stress intensity factor (at  $a_i$ , where the change of the crack propagation mechanism occurs) under various humidity environment are summarized in Tables 3, 4 and 5, respectively.

Figures 10 and 11 show the  $N_{int}/N_f(\%)$  as a function of  $N_f$  and stress amplitude in various environment. In dry air, more than 90% fatigue life was consumed in crack initiation, when life cycles exceed  $10^6$  cycles or stress amplitude smaller than 160 MPa. Even for specimen tested at 160 MPa in dry air, the crack initiation portion occupies 88.62% of total fatigue life. As a result of that, the crack propagation life can be reasonably ignored in dry air condition and micro-crack initiation life is nearly equals to total fatigue life and the maximum error is less than 12%. The value of  $N_{int}/N_f(\%)$  exhibited same trend that increasing stress amplitude corresponding to roughly linear decreased micro-crack initiation percentage. For instance, more than 99% fatigue life consumed in micro-crack initiation stage for specimen tested at 60 MPa in distilled water and 90 MPa in saturated air. However, more than 50% percentage fatigue life consumed in fatigue crack

**Table 3** Predicted fatigue crack initiation and propagation life and SIF in dry air

Stress (MPa)	Cycles to failure	$a_0$ (mm)	$a_i$ (mm)	a (mm)	$N_{a_0-a_i}$	$N_{a_i-a}$	$N_{int}$	SIF (MPa*m <sup>-1/2</sup> )
105	7.30E+07	0.032	2.94	3.67	1.81E+05 (0.25%)	5.98E+04 (0.08%)	7.28E+07 (99.67%)	6.56
105	4.26E+07	0.028	3.11	3.98	1.83E+05 (0.43%)	6.02E+04 (0.14%)	4.24E+07 (99.43%)	6.75
110	1.17E+07	0.031	2.81	3.44	1.65E+05 (1.41%)	5.03E+04 (0.43%)	1.15E+07 (98.16%)	6.72
110	5.96E+07	0.042	3.18	3.86	1.63E+05 (0.27%)	5.28E+04 (0.09%)	5.94E+07 (99.64%)	7.15
120	2.78E+06	0.036	3.50	4.25	1.39E+05 (5.01%)	3.93E+04 (1.41%)	2.60E+06 (93.58%)	8.18
120	8.55E+06	0.033	2.75	3.75	1.38E+05 (1.61%)	6.58E+04 (0.77%)	8.35E+06 (97.62%)	7.25
130	4.43E+06	0.034	2.53	3.33	1.17E+05 (2.64%)	5.31E+04 (1.2%)	4.26E+06 (96.17%)	7.53
130	3.08E+06	0.036	3.54	4.25	1.19E+05 (3.86%)	3.14E+04 (1.02%)	2.93E+06 (95.13%)	8.91
140	3.20E+06	0.028	2.43	5.27	1.02E+05 (3.18%)	1.06E+05 (3.31%)	2.99E+06 (93.51%)	7.95
140	4.96E+06	0.023	1.61	2.86	1E+05 (2.02%)	9.18E+04 (1.85%)	4.77E+06 (96.13%)	6.47
150	7.81E+06	0.032	2.99	3.76	8.89E+04 (1.14%)	3.0E+04 (0.38%)	7.69E+06 (98.48%)	9.45
150	1.59E+06	0.036	3.06	3.89	8.84E+04 (5.56%)	3.28E+04 (2.07%)	1.47E+06 (92.37%)	9.56
160	8.87E+05	0.029	2.88	3.52	7.84E+04 (8.84%)	2.25E+04 (2.54%)	7.86E+05 (88.62%)	9.89



**Table 4** Predicted fatigue crack initiation and propagation life and SIF in saturated air

Stress (MPa)	Cycles to failure	$a_0$ (mm)	$a_i$ (mm)	a (mm)	$N_{a_0-a_i}$	$N_{a_i-a}$	$N_{int}$	SIF (MPa*m <sup>-1/2</sup> )
90	4.91E+07	0.023	2.25	3.25	2.48E+05 (0.50%)	1.26E+05 (0.26%)	4.87E+07 (99.24%)	4.92
95	1.77E+07	0.025	2.12	2.31	2.20E+05 (1.25%)	3.05E+04 (0.17%)	1.74E+07 (98.58%)	5.04
100	5.03E+06	0.033	2.75	3.75	1.99E+05 (3.95%)	9.48E+04 (1.89%)	4.74E+06 (94.16%)	6.04
110	4.75E+06	0.02	2	3.5	1.66E+05 (3.49%)	1.22E+05 (2.56%)	4.46E+06 (93.95%)	5.67
110	1.84E+06	0.033	2.5	3.75	1.63E+05 (8.87%)	1.05E+05 (5.71%)	1.57E+06 (85.42%)	6.34
120	1.78E+06	0.015	1.25	2.71	1.38E+05 (7.75%)	1.47E+05 (8.26%)	1.49E+06 (83.98%)	4.89
130	1.48E+06	0.018	1.54	3.44	1.18E+05 (7.96%)	1.28E+05 (8.62%)	1.23E+06 (83.42%)	5.88
130	9.49E+05	0.01	1.75	3.25	1.22E+05 (12.86%)	7.17E+04 (7.56%)	7.55E+05 (79.58%)	6.27
140	1.42E+06	0.032	2.5	3.64	1.01E+05 (7.11%)	5.96E+04 (4.19%)	1.26E+06 (88.69%)	8.06
150	3.34E+05	0.036	1.96	3.39	8.57E+04 (25.67%)	8.7E+04 (26.04%)	1.61E+05 (48.29%)	7.65
150	3.50E+05	0.022	1.88	2.92	8.85E+04 (25.27%)	5.72E+04 (16.36%)	2.04E+05 (58.37%)	7.49
160	4.52E+05	0.025	1.92	2.31	7.72E+04 (17.09%)	2.37E+04 (5.25%)	3.51E+05 (77.67%)	8.08
170	2.48E+05	0.015	1.67	3.33	6.99E+04 (28.19%)	5.77E+04 (23.25%)	1.2E+05 (48.56%)	8.00

propagation stage when specimen tested at 140 MPa in water and 170 MPa in saturated air, respectively.

Also, Figs. 12 and 13 shows the variation of SIF in dry air, saturated air and distilled water environments, where the change of crack propagation mechanism occurs. Although

**Table 5** Predicted fatigue crack initiation and propagation life and SIF in distilled water

Stress (MPa)	Cycles to failure	$a_0$ (mm)	$a_i$ (mm)	a (mm)	$N_{a_0-a_i}$	$N_{a_i-a}$	$N_{int}$	SIF (MPa*m <sup>-1/2</sup> )
60	1.06E+08	0.032	2.53	4.23	5.5E+05 (0.52%)	4.27E+05 (0.40%)	1.05E+08 (99.08%)	3.48
70	1.20E+07	0.025	1.86	4.16	4.03E+05 (3.36%)	4.72E+05 (3.94%)	1.11E+07 (92.71%)	3.48
80	4.27E+06	0.016	1.67	2.92	3.15E+05 (7.37%)	2.25E+05 (5.26%)	3.73E+06 (87.37%)	3.77
90	2.36E+06	0.023	2.05	2.95	2.46E+05 (10.44%)	1.31E+05 (5.56%)	1.98E+06 (84.01%)	4.69
100	1.09E+06	0.02	1.82	3.18	2E+05 (18.33%)	1.54E+04 (14.11%)	7.36E+05 (67.56%)	4.92
110	5.83E+05	0.033	1.82	2.34	1.6E+05 (27.38%)	7.92E+04 (13.58%)	3.44E+05 (59.04%)	5.41
120	6.05E+05	0.024	1.76	2.63	1.37E+05 (22.62%)	8.89E+04 (14.70%)	3.79E+05 (62.68%)	5.80
130	3.46E+05	0.023	1.98	2.43	1.18E+05 (34.05%)	3.74E+04 (10.81%)	1.91E+05 (55.14%)	6.66
140	2.05E+05	0.026	2.12	2.36	1.01E+05 (49.39%)	1.78E+04 (8.67%)	8.6E+04 (41.94%)	7.43

**Fig. 10**  $N_{int}/N_f(\%)$  as a function of  $N_f$  in various environments

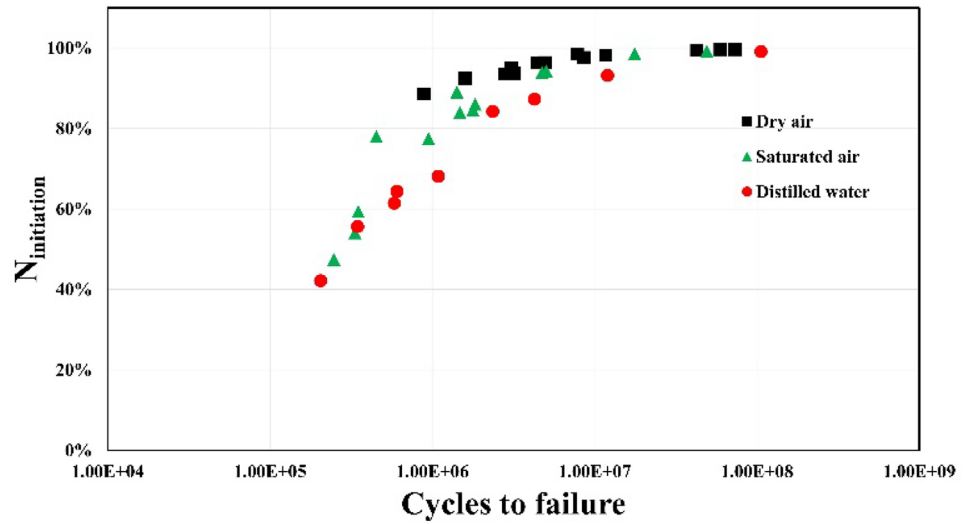


**Fig. 11**  $N_{int}/N_f(\%)$  as a function of stress amplitude in various environments

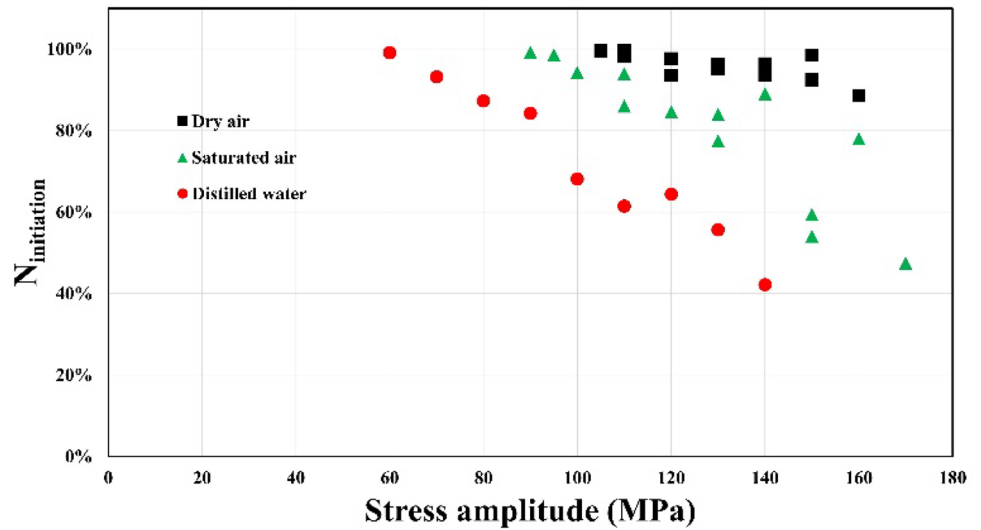


**Fig. 12** SIF versus cycles to failure in various environments

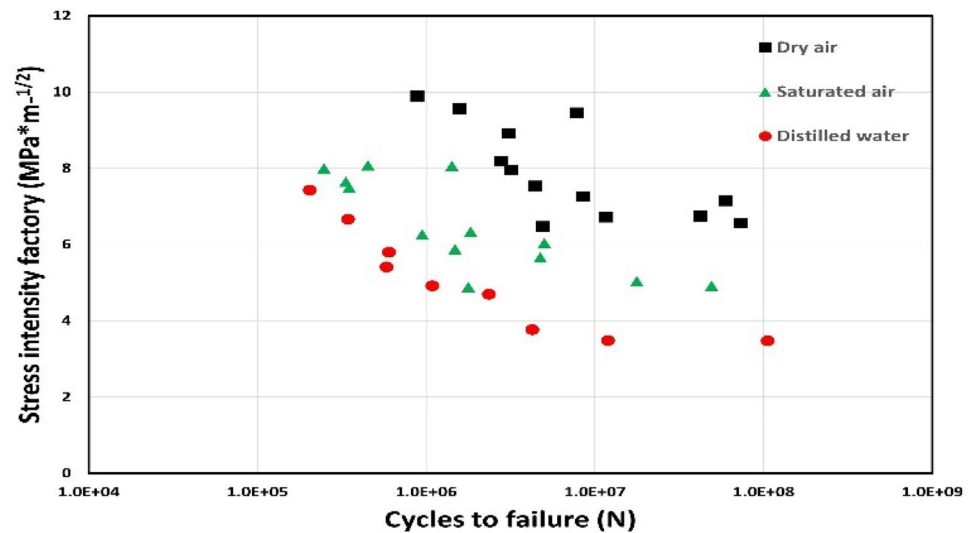
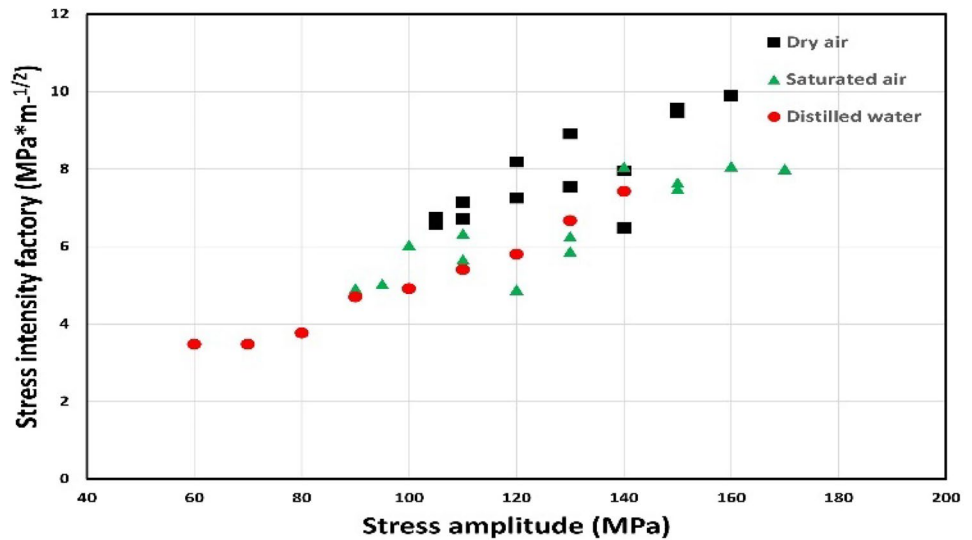


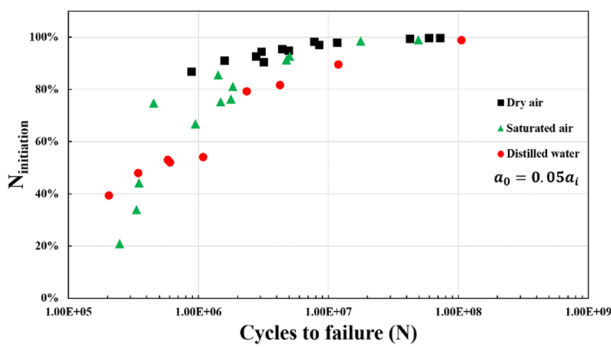
**Fig. 13** SIF versus stress amplitude in various environments



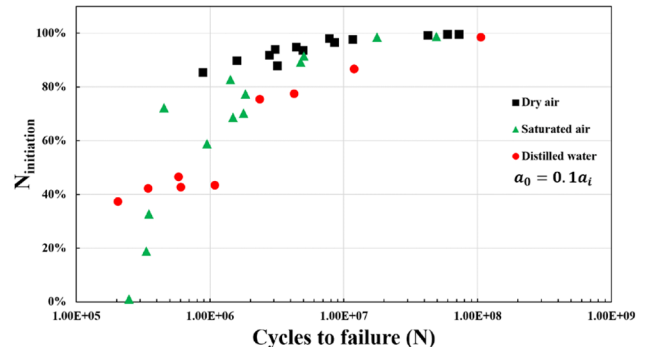
the value of SIF located in a certain range of 3.5 to 10  $MPa \cdot \sqrt{m}$  for these three environments, SIF in dry air is larger than in saturated air and distilled water conditions.

The transition point from short to long crack growth in an aluminum-environment system is often associated with

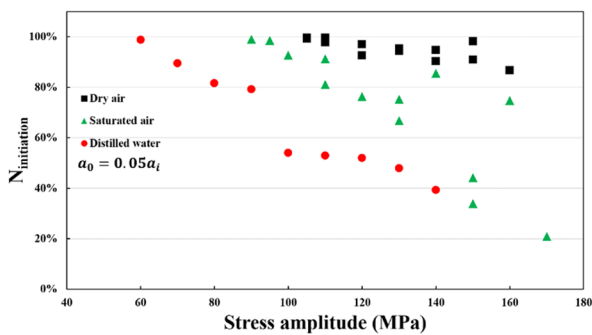
the presence of water vapor. It is assumed that the crack growth rate at this point also transitions from a slow crack growth rate to a fast crack growth rate. One contributing factor to crack growth rate acceleration is the presence of water vapor. This behavior used to be attributed to a crack



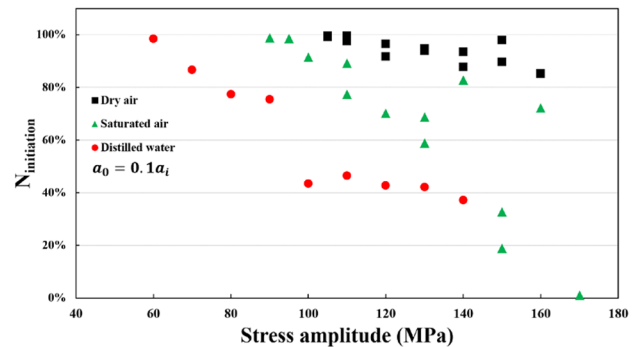
(a)



(b)



(c)



(d)

**Fig. 14** (a) and (b) are  $N_{int}/N_f(\%)$  as a function of  $N_f$  for  $a_0 = 0.05a_i$  and  $0.1a_i$  (c) and (d) are  $N_{int}/N_f(\%)$  as a function of stress amplitude for  $a_0 = 0.05a_i$  and  $0.1a_i$

tip hydrogen embrittlement mechanism proposed by Wei and co-workers [4, 27, 28]. According to the suggested model, the reaction kinetics in the aluminum-environment system play a crucial role in enhancing the crack growth rate in a saturated and distilled water environment. The crack growth rate can be divided into two components: crack growth rate caused by cyclic loading and crack growth rate induced by environmental humidity. In the short crack area, the crack growth rate is significantly enhanced by the humidity, resulting in a smaller value of the crack growth rate transition point ( $a_i$ ) in saturated air and distilled water compared to dry air conditions. On the other hand, in the long crack area, the crack growth rate is high, and the effect of humidity is minimized. Consequently, the stress intensity factor (SIF) in dry air conditions is higher than in saturated air and distilled water conditions.

Fatigue cracks typically initiate from casting defects such as pores, oxide inclusions, and segregation, among others. These defects tend to have larger sizes compared to the observed value of  $a_0$  in the present study. To investigate the effect of crack initiation size on the value of  $N_{int}/N_f(\%)$ ,  $a_0$  was also assigned as 0.05 and 0.1 times the value of  $a_i$ . The results are presented in Fig. 14. The findings in Fig. 14 align with the conclusions drawn from Figs. 10 and 11, indicating that a larger value of  $a_0$  results in a smaller portion of micro-crack initiation. For instance, when the crack initiation size was assumed to be 0.0167 mm ( $(0.01a_0)$ ), the value of  $N_{int}/N_f(\%)$  was found to be 47.44% when the specimen was tested at 170 MPa in saturated air. However, under the same conditions, when the crack initiation size was assigned as 0.0835 mm ( $(0.05a_0)$ ) and 0.176 mm ( $(0.1a_0)$ ), the corresponding total fatigue life was 20.96% and 1.12%, respectively.

In conclusion, humidity has a detrimental effect on the ultrasonic fatigue life of cast aluminum alloy, and the environmental impact should be carefully considered when using this fatigue data in component design. Moreover, as crack initiation constitutes a significant portion of the total fatigue life in the very high cycle fatigue (VHCF) regime, it is recommended to minimize potential defect sizes to enhance the ultrasonic fatigue performance of the material.

## Conclusions

The present study involved conducting ultrasonic fatigue tests on cast aluminum alloy AS7GU-T64 under different humidity conditions. The objective was to investigate the crack initiation mechanism and propose a probable explanation for the formation of facets. In addition, the crack lengths were characterized by measuring from the fracture surfaces. The fatigue life of the crack initiation stage, short crack growth, and long crack growth regions

was predicted using the Paris-Hertzberg-McClintock crack growth law. The main conclusions drawn from this work are outlined below:

1. Humidity has a detrimental effect on the ultrasonic fatigue life of cast aluminum alloy. Therefore, it is crucial to carefully evaluate the service environments when utilizing fatigue testing data in component design.
2. The observed facets on the fatigue fracture surfaces are identified as persistent slip bands, which formed by cyclic plastic strain accumulation during short crack propagation regime; these facets are confined within single grains with slip systems aligned with the maximum shear stress direction.
3. The distinction between crack initiation, short crack growth, and long crack growth areas is determined by analyzing the fracture morphology. Under dry air conditions, a significant portion of the ultrasonic fatigue life is consumed by crack initiation, making crack propagation life relatively negligible. The error associated with neglecting crack propagation life is found to be less than 12%.
4. The percentage of fatigue life attributed to crack initiation strongly depends on the humidity of the testing environment and the stress amplitude applied. The length of  $a_0$ , representing crack initiation size, also significantly influences this percentage.
5. Although the length of  $a_0$  does not alter the trend of  $N_{int}/N_f(\%)$  (crack initiation fatigue life over total fatigue life) versus fatigue cycles/stress amplitude, it does have a significant impact on the absolute values obtained.

**Acknowledgements** The author gratefully acknowledges the University Research Program at Ford Motor Company (URP2010-5055R) for financial support to this research.

**Funding** Ford Motor Company, URP2010-5055R, Wenkai Li.

**Data Availability** The data underlying this article are available in the article.

## Declarations

**Conflict of Interests** The authors declare that they have no known competing financial interests or personal relationships that could have appeared to influence the work reported in this paper.

## References

1. Stanzl-Tschegg SE, Mayer H (2001) Fatigue and fatigue crack growth of aluminium alloys at very high numbers of cycles. *Int J Fatigue* 23:231–237
2. Bathias C, Paris PC (2010) Gigacycle fatigue of metallic aircraft components. *Int J Fatigue* 32:894–897

3. Engler-Pinto Jr CC, Frisch Sr RJ, Lasecki JV, Allison JE, Zhu X, Jones JW (2006) High cycle fatigue of cast aluminum alloys at ultrasonic frequency. *SAE Trans* 541–547
4. Weir TW, Simmons GW (1980) A model for surface reaction and transport controlled fatigue crack growth. *Scripta Met* 14:357–364
5. Wei RP (1989) Environmentally assisted fatigue crack growth. *Adv Fatigue Sci Technol* Dordrecht: Springer Netherlands, 221–252
6. Stanzl-Tschegg SE, Schönbauer B (2010) Mechanisms of strain localization, crack initiation and fracture of polycrystalline copper in the VHCF regime. *Int J Fatigue* 32(6):886–893
7. Zhu X, Jones JW, Allison JE (2008) Effect of frequency, environment, and temperature on fatigue behavior of E319 cast aluminum alloy: Stress-controlled fatigue life response. *Metall and Mater Trans A* 39:2681–2688
8. Lados DA, Apelian D (2008) Relationships between microstructure and fatigue crack propagation paths in Al–Si–Mg cast alloys. *Eng Fract Mech* 75(3–4):821–832
9. Serrano-Munoz I et al (2016) Influence of surface and internal casting defects on the fatigue behaviour of A357–T6 cast aluminium alloy. *Int J Fatigue* 82:361–370
10. Le VD et al (2016) Simulation of the Kitagawa-Takahashi diagram using a probabilistic approach for cast Al-Si alloys under different multiaxial loads. *Int J Fatigue* 93:109–121
11. Paris PC, Marines-Garcia I, Hertzberg RW, Donald JK. In: Tatsuo Sakai (Ritsumeikan University), Yasuo Ochi (University of Electro-Communications) (Eds.), Proceedings of the International Conference on Very High Cycle fatigue III (VHCF-3), Rohm Plaza, Ritsumeikan University, Kusatsu, Japan, sponsored by Soc Mater Sci (JSMS) and, Res Group Stat Aspect Strength (RGSAMS) and Ritsumeikan University, September 2004
12. Nakasone T, Hara H. In: Tatsuo Sakai (Ritsumeikan University), Yasuo Ochi (University of Electro-Communications) (Eds.), Proceedings of the International Conference on Very High Cycle fatigue III (VHCF-3), Rohm Plaza, Ritsumeikan University, Kusatsu, Japan, sponsored by Soc Mater Sci (JSMS), and Res Group Stat Aspect Strength (RGSAMS) and Ritsumeikan University, September 2004
13. Omata. In: Tatsuo Sakai (Ritsumeikan University), Yasuo Ochi (University of Electro-Communications) (Eds.), Proceedings of the International Conference on Very High Cycle fatigue III (VHCF-3), Rohm Plaza, Ritsumeikan University, Kusatsu, Japan, sponsored by Soc Mater Sci (JSMS) and, Res Group Stat Aspect Strength (RGSAMS) and Ritsumeikan University, September 2004
14. Mayer H (2016) Recent developments in ultrasonic fatigue. *Fatigue Fract Eng Mater Struct* 39(1):3–29
15. Mayer H (2006) Ultrasonic torsion and tension–compression fatigue testing: Measuring principles and investigations on 2024–T351 aluminum alloy. *Int J Fatigue* 28(11):1446–1455
16. Bathias C (2006) Piezoelectric fatigue testing machines and devices. *Int J Fatigue* 28(11):1438–1445
17. Ryan KJ (2003) Estimating expected information gains for experimental designs with application to the random fatigue-limit model. *J Comput Graph Stat* 12(3):585–603
18. Stanzl SE, Mayer HR, Tschegg EK (1991) The influence of air humidity on near-threshold fatigue crack growth of 2024–T3 aluminum alloy. *Mater Sci Eng A* 147(1):45–54
19. Miao J, Pollock TM, Jones JW (2012) Microstructural extremes and the transition from fatigue crack initiation to small crack growth in a polycrystalline nickel-base superalloy. *Acta Mater* 60(6–7):2840–2854
20. Tiryakioğlu M, Campbell J, Nyahumwa C (2011) Fracture surface facets and fatigue life potential of castings. *Metall and Mater Trans B* 42:1098–1103
21. Zhu X et al (2006) Effects of microstructure and temperature on fatigue behavior of E319–T7 cast aluminum alloy in very long life cycles. *Int J Fatigue* 28(11):1566–1571
22. Lin TH, Liu HQ, Liang NG (2003) A micromechanical theory of fatigue crack initiation of an aluminum single crystal. *Int J Fatigue* 25(9–11):871–876
23. Murakami Y, Kodama S, Konuma S (1989) Quantitative evaluation of effects of non-metallic inclusions on fatigue strength of high strength steels. I: Basic fatigue mechanism and evaluation of correlation between the fatigue fracture stress and the size and location of non-metallic inclusions. *Int J Fatigue* 11(5):291–298
24. Standard Test Method for Measurement of Fatigue Crack Growth Rates. ASTM 2000. E 647–00
25. Hertzberg RW, Vinci RP, Hertzberg JL (2020) Deformation and fracture mechanics of engineering materials. John Wiley & Sons
26. Marines-Garcia I et al (2007) Fatigue crack growth from small to long cracks in very-high-cycle fatigue with surface and internal “fish-eye” failures for ferrite-perlitic low carbon steel SAE 8620. *Mater Sci Eng A* 468:120–128
27. Wei RP, Simmons GW (1981) Recent progress in understanding environment assisted fatigue crack growth. *Int J Fract* 17:235–247
28. Wei RP (2002) Environmental considerations for fatigue cracking. *Fatigue Fract Eng Mater Struct* 25(8–9):845–854

**Publisher's Note** Springer Nature remains neutral with regard to jurisdictional claims in published maps and institutional affiliations.

Springer Nature or its licensor (e.g. a society or other partner) holds exclusive rights to this article under a publishing agreement with the author(s) or other rightsholder(s); author self-archiving of the accepted manuscript version of this article is solely governed by the terms of such publishing agreement and applicable law.